A 0.5-V 3.6/5.2 GHz CMOS Multi-Band LC VCO for Ultra Low-Voltage Wireless Applications

Burak Çatlı and Mona M. Hella

Electrical, Computer, and Systems Engineering Department
Rensselaer Polytechnic Institute Troy, New York 12180-3590
Email: {catlib, hellam}@rpi.edu

***Abstract*—In this paper, an ultra low-voltage multiband CMOS VCO based on tunable band-limited negative resistance approach is presented. The proposed technique eliminates the need for switching elements that are connected directly to the tank and limit the tuning range and phase noise performance. The oscillator draws a current of 6mA from 0.5V supply with a phase noise of -117dBc/Hz at 1MHz offset from 3.6GHz carrier. For the high frequency band, it draws 4mA from the same supply with a phase noise of -117dBc/Hz at 1MHz offset from 5.2GHz carrier.**

I. Introduction

The increasing consumer demand for multi-functional portable devices has forced industry to seek almost the ideal radio: low-power, low-voltage and multistandard. New standards such as software defined radios (SDR) and cognitive radios (CR) will reshape the wireless market in the next few years. The common features of such systems are frequency agility, whether wideband and/or multiband operation and reconfigurability to adapt to different modulation standards. In order to support the frequency agility property, multi-band frequency generation circuits are required. A number of techniques have been proposed to generate multi-band signals. These techniques can be classified into three main categories: switched resonator tanks [1], post processing of the generated signal [2] and micro-electro-mechanical systems MEMS-based solutions[3]. In the first category, the resonance frequency of an oscillator tank is modified by adding L and C elements to the tank via MOS switches, which reduces the tuning range and increases phase noise. In the second category, the generated signal by a single band oscillator is processed by frequency dividers, mixers and passive filters. The obvious disadvantage of this technique is high power and area consumptions with the added contribution of the large post processing circuitry. Approaches using MEMS-based RF switches require additional fabrication steps which increases the cost and affects the reliability of the RF solution.

In this paper, we propose a band limited negative resistance based multiband VCO. In this topology, we move the band switching task from the tank to the negative resistance portion of the oscillator. Thus, the frequency selectivity properties of the tank are not degraded by the additional switching which is normally added to the tank to perform multiband operation. To the best knowledge of the authors', this is the first circuit level multiband VCO design that eliminates the role of the tank in the band switching mechanism and treats the tank as a fixed multiband resonator, whose frequencies are turned ON/OFF by changing the amplitude and frequency range of the negative resistance circuit.

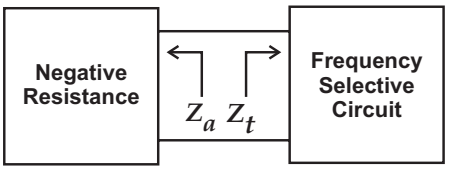

Fig. 1. Negative resistance oscillator

II. Basic Concept

Oscillators can be modeled using the negative resistance model shown in Fig. 1. The *necessary* conditions for starting oscillation are: 1- The frequency selective network must have at least one resonance frequency 2- The active circuit should provide *enough* negative resistance at that resonance frequency to compensate for the loss of the tank.

If we consider a multi-band resonator which has two resonance points located at ω_1 and ω_2 as shown in Fig. 2, we see that the resonator needs enough negative resistance at each resonance frequency to start an oscillation. If a regular negative resistance circuit is employed, such as a cross-coupled negative resistance cell, it will provide a broadband negative resistance from DC to very high frequencies beyond the value of ω_2. This will provide concurrent oscillations satisfying the oscillation conditions at each band. However, if the bandwidth of the negative resistance is limited to a narrow frequency range that can be centered around each frequency separately, the oscillation condition can be provided for only one band (ω_1), while not provided for the other band, (ω_2). When band-switching is required, the center frequency of the band-pass characteristic of the negative resistance can be moved to a different frequency band. Fig. 2 illustrates the band switching mechanism by plotting the real component of the tank impedance ($Re[Z_t]$) and of the negative resistance element ($Re[Z_a]$) as a function of frequency for dual band scenario. The tank impedance has a fixed dual resonance characteristics, while the negative resistance unit provides a

978-1-4244-1684-4/08/$25.00 ©2008 IEEE

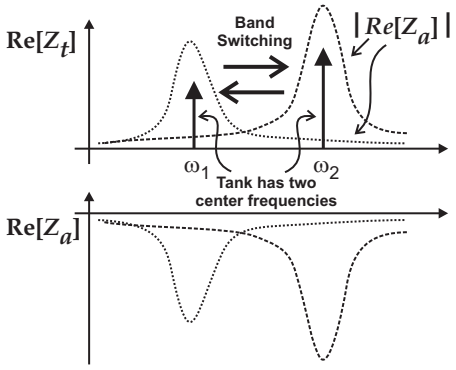

Fig. 2. Band switching mechanism by moving the negative resistance ($Re[Z_a]$) from one band to another

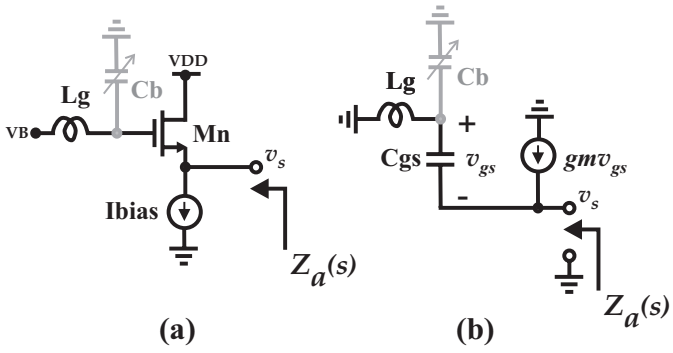

Fig. 3. The simple (bold) and band limited tunable negative resistance (with the addition of the capacitor in gray) (a) Transistor level schematic (b) Equivalent circuit

negative resistance within a limited frequency range around a single frequency (ω_1 or ω_2) that can be switched to the other frequency based on a control signal as will be discussed in section III. Note that, the proposed technique does not reconfigure the frequency selective network, and thus maintains the tuning range and phase noise performance without additional switching loss.

Although the concept is explained on the *necessary* conditions, since the oscillation process is a large signal phenomenon, other tools, such as Nyquist diagram and root-locus analysis are essential to guarantee the oscillation conditions[4].

III. Band-Limited Negative Resistance

A negative resistance cell can be realized by connecting an inductor L_g to the gate of a MOS transistor as shown Fig. 3a. The impedance seen into the source, $(Z_a(\omega))$, can be calculated using the simple equivalent circuit in Fig. 3b *ignoring all other parasitic components*:

$$Z_a(\omega) = \frac{gm\left(1-\omega^2 CgsLg\right) + j\left(\omega^3 Cgs^2 Lg - \omega Cgs\right)}{gm^2 + \omega^2 Cgs^2} \tag{1}$$

As a result of this first-order analysis, we can state that the real part of the source impedance, $Re(Z_a(\omega))$, starts to become negative at frequency ω_x where

$$\omega_x = \frac{1}{\sqrt{LgCgs}} \tag{2}$$

Unlike the traditional cross-coupled negative resistance configuration which exhibits negative resistance starting from DC to very high frequencies in a broadband form, the proposed circuit in Fig. 3 will start to exhibit negative resistance after a certain frequency, ω_x and will maintain this negative resistance behavior for a finite frequency range. With the addition of a tunable gate capacitor (tunable capacitor Cb shown in Fig. 3), the impedance looking at the source of the MOS transistor will cease to become negative at frequency ω_p (upper frequency of the negative resistance range). The modified impedance $Z_a(\omega)$ after the addition of Cb can be found from the following equation.

$$Z_a(\omega) = \frac{\begin{array}{c}(gm(1-w^2(Cb+Cgs)Lg) \\ +j(w^3 Cgs(Cb+Cgs)Lg - wCgs))\end{array}}{gm^2 + w^2 Cgs^2 - w^2 LgCb(gm^2 + w^2 Cgs^2)} \tag{3}$$

and the frequency limits of the negative resistance range, ω_x and ω_p, can be rederived as

$$\omega_x = \frac{1}{\sqrt{Lg(Cgs+Cb)}} \tag{4}$$

$$\omega_p = \frac{1}{\sqrt{LgCb}} \tag{5}$$

(4) and (5) show the effect of Cb over negative resistance bandwidth. Fig. 4 shows the simulated real part of the source impedance for the proposed circuit at different values of Cb, compared to a simple negative resistance topology. It is clear from the figure that the addition of Cb allows the negative resistance band to move from one frequency range to the other, enabling band switching

IV. Circuit Design

A. Multiband Resonator

A fourth-order LC circuit shown in Fig. 5 is used to create the dual-band resonator. A double-tuned transformer [5] could have also been selected as dual-band resonator.

The impedance characteristic of the resonator can be given as in the following:

$$Z_t(\omega) = \frac{j\omega L_1(1-\omega^2 C_2 L_2)}{1-\omega^2(C_1L_1 + C_2(L_1+L_2)) + \omega^4 C_1C_2L_1L_2} \tag{6}$$

The resonator is a combination of a parallel (L_1, C_1) and a series resonance circuit (L_2, C_2). The selection of the two resonance frequencies is limited by practical values of (L_1, C_1, L_2, C_2). To illustrate this limitation, L_2/L_1 is plotted for different C_1/C_2 ratios as a function of ω_2/ω_1 in Fig. 6. The figure shows that as the resonance frequencies gets closer, L_2/L_1 increases. It is obvious that high L_2/L_1 ratios cause implementation problems and increase the die area. Although

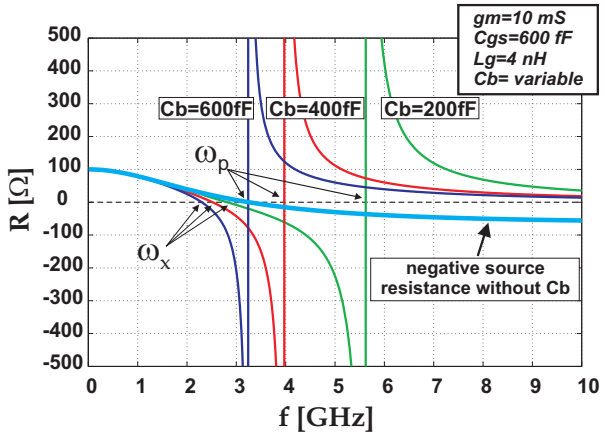

Fig. 4. Illustration of negative resistance bandwitdh control for sample parameter set

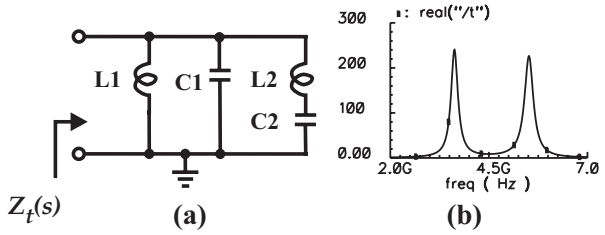

Fig. 5. 4^{th} order LC resonator and its simulated real impedance.

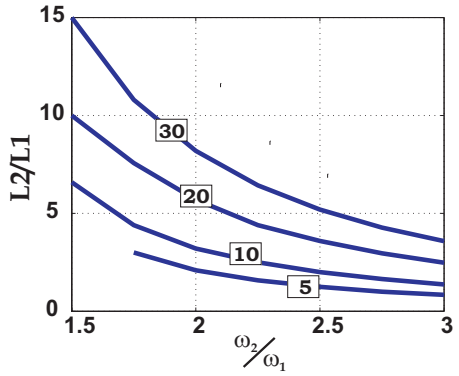

Fig. 6. L_2/L_1 ratio as a function of C_1/C_2 and ω_2/ω_1

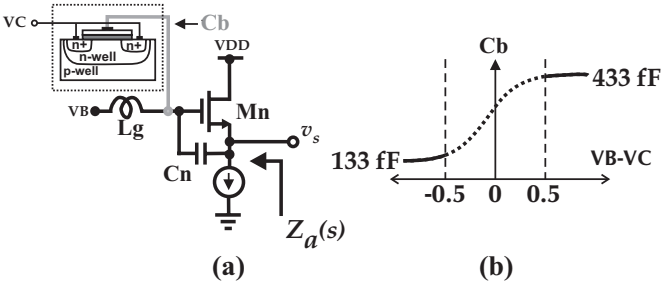

Fig. 7. The capacitor Cb is implemented as an accumulation mode varactor. By changing $VB-VC$ potential difference, the accumulation mode varactor is slide to one of the two *flat* states of the capacitance characteristic to accomplish band switching

this ratio can be decreased by selecting lower values C_1/C_2, this may not help in some cases. For example, if the ratio $\omega_2/\omega_1 = 1.5$ selected, it is seen from Fig. 6 that there is no solution for C_1/C_2=5. The case may be more dramatic for the ω_2/ω_1 values less than 1.5. While the ω_2/ω_1 of 1.5 ratio is not significant in the frequency range below 10GHz, as we move to the mm-wave bands, this ratio can be equivalent to 10GHz band separation.

In the current resonator, low-band and high-band center frequencies are selected as 3.6 and 5.2 GHz. L_1=0.92nH, L_2=5.57nH, C_1=1.677pF and C_2=293fF are the selected design parameters for the tank. C_1 and C_2 are calculated from (6), however their values are readjusted to compensate for the large substrate parasitic capacitance of L_2=5.57nH.

B. Negative Resistance

The actual negative resistance cell employed in the oscillator is shown in Fig. 7. The transistor M_n is sized to satisfy the required negative resistance bandwidth and amplitude as well as phase noise specifications. For the oscillator to operate at frequency (ω_1), the lower frequency limit of the negative resistance , (ω_x) should be selected lower enough than (ω_1) to guarantee oscillation. From (4),this can be done by increasing the aspect ratio for the MOS transistor M_n to increase Cgs. However, if the aspect ratio is selected arbitrarily high, the higher gm will degrade the phase noise severely due to the effect of drain noise. For example, for a 3 nH gate inductor and an aspect ratio of 224/0.12, the oscillation is guaranteed at the expense of -90 dBc/Hz at 1MHz offset from a 3.6 GHz carrier signal. On the other hand, if the aspect ratio is reduced gradually, the flicker noise becomes dominant over the phase noise performance. As a result, a combined solution is required to optimize both negative resistance and phase noise performance. An aspect ratio of 150 is selected to keep the gm low, however a channel length higher than minimum feature size ($L = 0.5\mu m$) is selected to keep the overall WL high and reduce the contribution of flicker noise to phase noise. In addition to this, an additional MIM capacitor $Cn = 500fF$ is connected between gate and source terminal as shown in Fig. 7 to guarantee oscillation.

C. The VCO

The simplified schematic of the VCO is shown in Fig. 8. The oscillator is designed in IBM $0.13\mu m$ CMOS technology. The inductors are created by stacking two top metal of the process and MIM capacitors are used to realize the capacitors. The oscillator is capable of operating with and without of a tail current source with an appropriate selection of bias voltage VB. When the current source is enabled, the output signal swings a certain DC level and its amplitude can be adjusted by the tail current.However, when the current source is disabled for low-voltage operation and center tap is connected ground, the output signal swings around 0 V DC level. To avoid any forward biased diode problem at source, triple-well nMOS transistors are used for $Mn1$ and $Mn2$, and their source

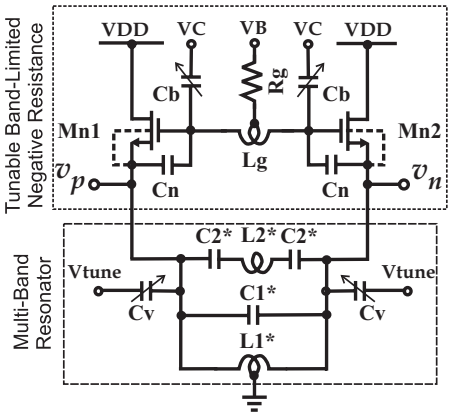

Fig. 8. Schematic of the multiband VCO

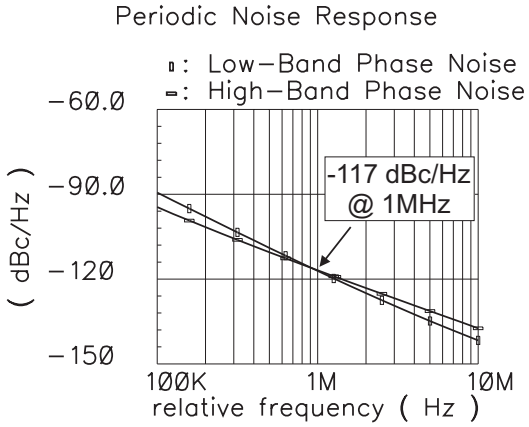

Fig. 9. Phase noise simulation results

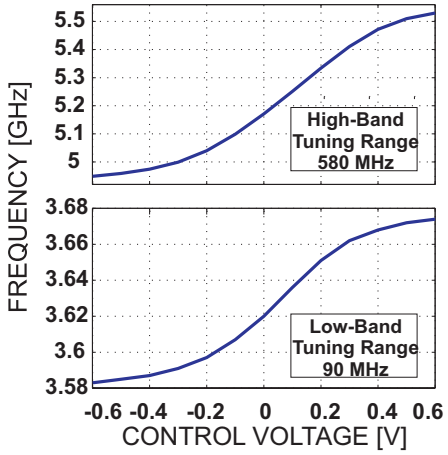

Fig. 10. Frequency tuning characteristics of the VCO

terminals are connected to body terminals.

The frequency planning of the VCO is based on actual SDR system and the center frequencies are selected as 3.6 and 5.2 GHz [6]. With the addition of the frequency dividers as in [6], the oscillator is able to support most of the communication standards within SDR range (800MHz-6GHz) with a single VCO compared to two stand-alone VCOs as in [6]. The frequency tuning is based on the accumulation mode varactors. While the coarse tuning (band-switching) is performed by accumulation mode varactors (Cb) switching to one of the states(133fF or 433fF) shown in Fig. 7, the fine-tuning (in-band tuning) is performed by the other accumulation mode varactor set (Cv) directly connected to the resonator. In fact the calculated C_1=1.677pF is formed by (Cv) and MIM capacitor C_1^*.The gate biasing VB is provided through a high impedance (Rg) to suppress any even mode oscillation.

V. Simulation Results

The oscillator is nominally supplied by 0.5V VDD with the bias current adjusted by gate bias voltage VB. Fig. 9 shows the phase noise performance of the VCO at low and high bands. The oscillator draws a current of 6mA from 0.5V supply with a phase noise of -117dBc/Hz at 1MHz offset from 3.6GHz carrier. For the high frequency band, it draws 4mA from the same supply with a phase noise of -117dBc/Hz at 1MHz offset from 5.2GHz carrier.

The tuning characteristics of the VCO is shown in Fig. 10. The high-band tuning range is much higher than the low-band tuning range due to the asymmetrical nature of the tank. Additionally, series connection of C_2 to L_2 prevents the use of C_2 as varactors for additional tuning.

The VCO is simulated keeping its bias voltage constant but reducing the supply voltage VDD gradually down to $300mV$. For $VDD = 300mV$, the phase noise is -112.7 dBc/Hz and -108.3 dBc/Hz at 1 MHz frequency offset from the specified carrier frequencies for low-band and high-band, respectively.

VI. Conclusion

An ultra-low voltage multiband LC VCO is presented. The oscillator uses a tunable band-limited negative resistance mechanism to perform the band-switching, which is different from traditional switched resonator approach. Thus, it avoids the drawbacks of lossy switches that deteriorates phase noise and tuning range. The oscillator has a maximum power consumption of 3mW with reasonable performance compared to published multi-band oscillators, while operating at a supply voltage as low as 0.5V.

References

[1] S.-M. Yim and K. K. O, "Switched resonators and their applications in a dual-band monolithic CMOS LC-tuned VCO," *IEEE Transactions on Microwave Theory and Techniques*, vol. 54, no. 1, pp. 74–81, Jan. 2006.

[2] H. Shin, Z. Xu, and M. F. Chang, "A 1.8-V 6/9-GHz reconfigurable dual-band quadrature LC VCO in SiGe BiCMOS technology," *IEEE Journal of Solid-State Circuits*, vol. 38, no. 6, pp. 1028–1032, June 2003.

[3] R. Gaddi and et. al., "Reconfigurable mems-enabled lc-tank for multi-band cmos oscillator," in *IEEE MTT-S Int. Microw. Symp. Dig*.

[4] N. M. Nguyen and R. G. Meyer, "Start-up and frequency stability in high-frequency oscillators," *IEEE Journal of Solid-State Circuits*, vol. 27, no. 5, pp. 810 – 820, May 2005.

[5] B. Çatlı and M. M. Hella, "A dual band, wide tuning range cmos voltage controlled oscillator for multi-band radio," in *IEEE Radio Frequency Integrated Circuits (RFIC) Symp. Dig*, Honolulu, Hawaii, June 2007, pp. 595–598.

[6] R. Bagheri and et. al., "An 800-MHz 6-GHz Software-Defined Wireless Receiver in 90-nm CMOS," *IEEE Journal of Solid-State Circuits*, vol. 41, no. 12, pp. 2860–2876, Dec. 2006.